The Eurasia Proceedings of Science, Technology, Engineering & Mathematics (EPSTEM)
ISSN: 2602-3199

The Eurasia Proceedings of Science, Technology, Engineering and Mathematics (EPSTEM), 2025

Volume 37, Pages 720-735

ICEAT 2025: International Conference on Engineering and Advanced Technology

Characterization and Properties of Reaction Majnoon Field Rock Stone with Carbon Dioxide

Ibrahem I. Moslam
University of Al-Qadisiyah

Ali A. Jazie
University of Al-Qadisiyah

Rafid K. Abbas
University of Al-Qadisiyah

Abstract: Under simulated in-situ settings (T = 60°C, P = 74bar, 87-day batch tests), representative Majnoon rock stone samples from the Majnoon Field (Iraq) were analyzed to study geo-chemical responses arising from CO2 exposure. Albite, calcite, quartz, feldspars, clinochlore, dolomite, kaolinite, muscovite, orthoclase, and ankerite were among the mineral phases found by XRD examination. Because of the dissolution of minerals, the CO2 interaction caused the brine to become acidic and enriched in cations. Elements including silicon, oxygen, sodium, calcium, chlorine, carbon, fluorine, magnesium, and aluminum were verified by SEM and EDX. Prior to the reaction, kaolinite had the lowest phase abundance (~0.77 wt%) and calcite the greatest (~67 wt%). After the reaction, orthoclase dramatically dropped (~0.41 wt%), but calcite remained dominant (~69.67 wt%).. The highest reaction percentages were recorded for albite (~82%) and orthoclase (~84%), while kaolinite and quartz showed the lowest (~14% and ~24%, respectively). CO_2 addition caused a pH drop and led to calcium concentrations reaching ~1009 mg/L within five days. The study comes to the conclusion that carbonate dissolution, phyllosilicate (clinochlore/muscovite) hydrolysis, and montmorillonite precipitation are all involved in the CO2–Majnoon rock stone interaction.

Keywords: Majnoon field rock stone, Carbon dioxide, X-ray diffraction, Scanning electron microscope, Rock stone reaction

Introduction

Carbon capture and storage (CCS) is a technique used for climate change reduction and sustainable transitions. It has been studied for a long time and was considered a method for reducing atmospheric carbon concentrations in 1977 (Evar et al., 2012). CCS includes catching CO2 from power plants or different manufacturing places (International Energy Agency, 2021). The carbon dioxide is compressed and transferred to deep geological formations for storage (International Energy Agency, 2022). Other sources for capturing carbon dioxide include the atmosphere and bioenergy processes. Captured carbon dioxide can be used directly in industry rather than being stored (Bruhn et al., 2016).

The threat of carbon dioxide emissions emerged during the Third Industrial Revolution, driven by a significant surge in CO_2 output. As a result, carbon dioxide levels were projected to reach 570 parts per million, potentially causing a sea level rise of 3.8 degrees and an increase in global temperature of roughly 1.9 degrees Celsius meters (International Energy Agency, 2022). The world's largest emitters of carbon dioxide are China and the United

States (Atreya, 2022). Among the major contributing sectors, power generation ranks first, followed by the manufacturing sector, which accounts for 22% of emissions in 2019 (Atreya, 2022), as shown in Figure 1. The transportation sector is the third largest source of CO_2 emissions. Figure 2 (Bureau of Environment Tokyo Metropolitan Government, 2019) shows Energy-derived CO2 emissions by country (2019).

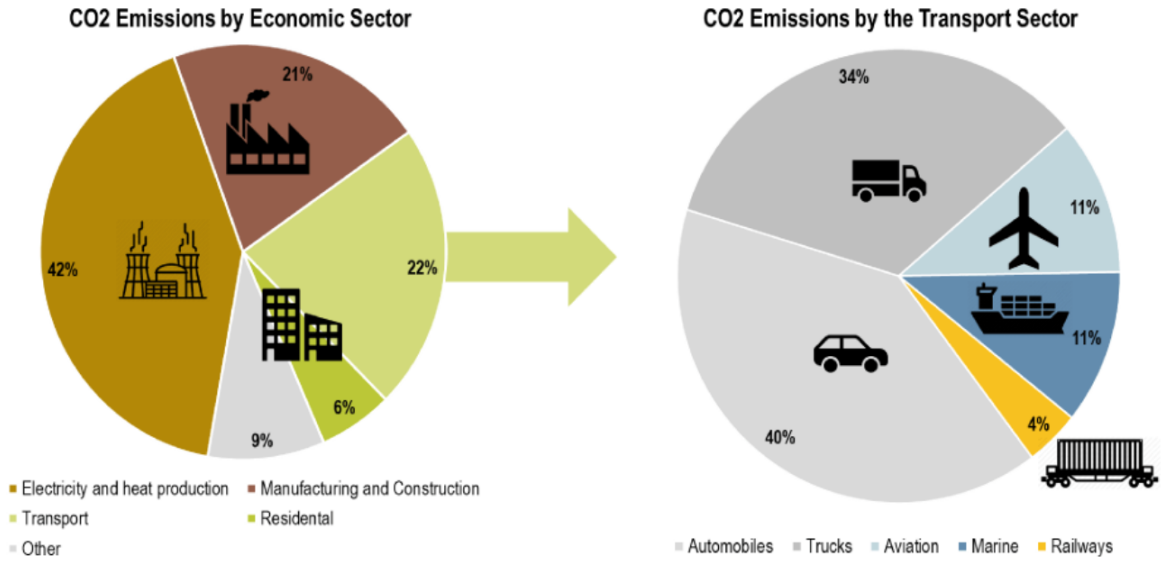

Figure 1. Global CO2 emission by sectors in 2019 (Atreya, 2022)

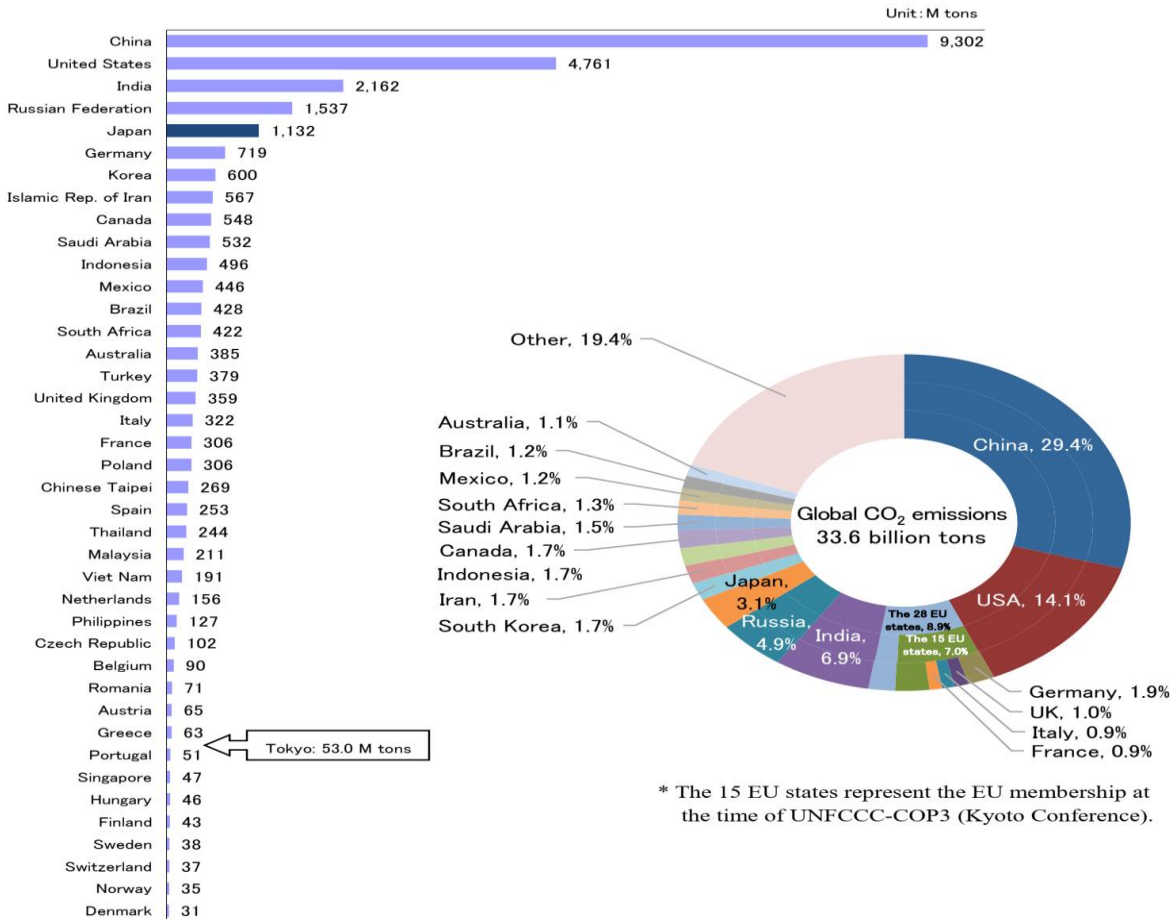

Figure 2. Energy-derived CO2 emission by country (2019)

In recent years, the world has increasingly embraced carbon capture and storage (CCS) as a key strategy for reducing carbon dioxide emissions. The International Energy Agency's 2022 Sustainable Development Plan set

ambitious targets to lower CO_2 emissions (International Energy Agency, 2022). Supporting this initiative, the European Commission adopted CCS as part of its policy framework for achieving carbon neutrality (European Commission, 2024). CCS plays a vital role in addressing climate change, serving the diverse interests of society by making significant contributions to global climate goals (Climate Action, 2023).

Injecting CO2 into subterranean deep brine water or in depleted oil and gas reserves are two ways to store carbon dioxide. Temperatures above 31.1°C and pressures above 7.4 MPa are usually necessary for CO_2 to exist as a stable supercritical fluid (CO_2) at depths larger than one kilometer. When CO2 is only injected, it is kept underground through processes such mineral capture, dissolvable trapping, capillary trapping, and constitutional trapping (De Silva et al., 2015; Wigand et al., 2008).

Furthermore, choosing the right tanks and cover rocks is difficult and necessitates thorough geological analyses. Before verifying the basin's suitability for storage, these investigations must assess its characteristics, such as porosity, permeability, geometry, capacity, and mineralogy. The integrity of reservoirs and the effectiveness of trapping may be impacted by the many geochemical reactions that are triggered by the presence of sCO_2 in geological formations. Pore water acidification, elementary mineral disintegration, subaltern stage deposition, and changes in porosity and permeability are some of these processes (Black et al., 2014; Gaus, 2010). To ascertain if such modifications increase or decrease the reservoir's capacity to store CO2, a thorough site-specific assessment is necessary.

Numerous scientists have investigated the potential for CO2 storage in both local CO2 storage stations (Wigand et al., 2008) and laboratory (Alemu et al., 2011; García-Rios et al., 2013; Huq et al., 2012). The research includes granites (Lin et al., 2008), shales (Sorensen et al., 2009), basalts (Van Pham et al., 2011), sandstones and limestones (García-Rios et al., 2013 The batch reactors were employed in this research, where a steady amount of sandstone and brine solution was positioned in a vessel and compressed with carbon dioxide to permit the interaction to take place over time (Lu et al., 2013; Rathnaweera et al., 2016).

In this work, representative Majnoon rock stone samples from the Majnoon Field, west of Basra, Iraq, are examined for possible mineralogical development upon exposure to brine saturated with supercritical CO2. A constant CO2 pressure of 74 bar and a temperature of 60 °C were established for the experiment. The resulting data were used to identify and characterize geochemical reactions occurring under these conditions.

Study Area

Majnoon field Lies in southern Iraq close to Basra and near the Iranian boundary, as shown in Figure 3. The field is known for its great hydrocarbon stores and complicated working environment, figured by both geographical and technical defiance. founded by the Brazilian Co. Braspetro, the expansion of the field extension from 1975 to 2021. Majnoon is assessed to include between 12 and 30 billion barrels of oil in reserves. Currently, output ability extends from nearly 200,000 to 240,000 barrels per day (bpd), with the potential to exceed 1 million bpd during further improvement. The field extends upon a space of approximately 12,000 to 15,000 Km^2.

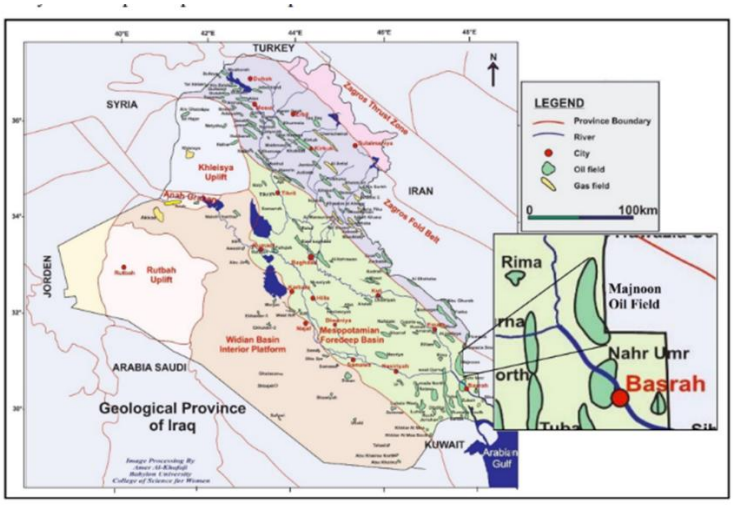

Figure 3. Location of Majnoon, the giant Iraqi field (Al-Ameri et al., 2011)

Materials and Methods

Materials

The rock stone specimens employed in the present empirical research were gained from the Majnoon oil field, one of the hugest oil fields in the global. The sedimentary formations surrounding the Majnoon Oilfield are part of the Mesopotamian Basin, a main geological characteristic in southern Iraq. This basin includes a heavy sequence of sedimentary coats that have stacked through millions of years, foremost through the Mesozoic and Cenozoic eras. It is estimated to be one of the Middle East's most hydrocarbon-privileged regions, owing to its favorable geological history and structural setting.

Experimental Setup and Procedure

The degree of CO2/water/rock interactions can be determined by analyzing extracted fluids and solid residues. This experimental technique is ideal for predicting the types and orientations of fast CO2/water/rock interactions because it provides the benefits of exact control over the laboratory conditions and relative simplicity. Additionally, flow-through experiments offer a more accurate model of reactive transport mechanisms and subsurface conditions (Huq et al., 2015; Luquot et al., 2012; Bateman et al., 2005; Galarza et al., 2013).

A grain size of 300 μm was chosen to be evaluated after each Majnoon rock stone sample was carefully crushed and sieved. The size of 300 μm was selected because it was both rough enough to enable mineralogical characterization and soft enough to give enough surface area for observable reactions throughout the empirical period. The Majnoon rock stone granules were filtered using a Büchner funnel equipped with Whatman No. 1 filter paper after being swilled with acetone to remove particles. In order to maintain a fluid:rock mass ratio of 10:1, 20 g of the cleaned, grained Majnoon rock stone was weighed and combined with 200 ml of a roughly 0.5 M NaCl mixture.

Epoxy resin was used inside the carbon steel reaction tank to reduce corrosion and prevent contamination. To facilitate the efficient blending of the liquid and solid phases, a magnetic mixer was used; to protect the pellets from mechanical damage, the mixer was housed in a tiny frame that was placed just above the container's base. A dunk pipe extending to the undermost of the container permitted the retraction of hydrous specimens during an experiment. After assembly, the vessel was warmed up in a propeller-supported Binder furnace to 60 °C, with industrialist information indicating temperature inconstancy of lower than ±0.5 °C.

The salinity used in the experiment, approximately equivalent to that of seawater, was selected based on previous studies (Baraka, 2015; De Silva et al., 2015; Zhang and Pu, 2011). To guarantee effective rock/fluid interaction, the mixture was mixed using a magnetic stirrer for 2 minutes each 4 hours. This periodical mixing nearly reduced mechanical abrasion of the Majnoon rock stone grains while still promoting adequate mixing of reactants throughout the test. Through the first thirty-seven days, the Majnoon rock stone and seawater were permitted to partly equilibrate at CO_2-free circumstances. Before each hydrous specimen combination, 1–1.5 ml of fluid was left and rejected to flush and clean the sampling lines. Typically, 10 ml of sample was compiled per extraction. By day 37, two brine samples had been collected. Following this, the reactor headspace was depressurized and flushed with excess CO_2 at 60 °C. After flushing, the CO_2 pressure was increased and maintained at 74 bar (7.4 MPa), corresponding to supercritical CO_2 conditions.

Under these conditions, ten additional brine samples were collected throughout the remainder of the experiment. During each sampling, the CO_2-rich brine was allowed to degas into a sterile syringe. A schematic of the batch reactor setup is provided in Figure 4.The rock stone specimens employed in the present empirical research were gained from the Majnoon oil field, one of the hugest oil fields in the global. The sedimentary formations surrounding the Majnoon Oilfield are part.

The unavoidable loss of CO_2 during sampling can significantly affect rapidly responding geochemical parameters, such as pH, which may change if samples are left to equilibrate over time. To minimize such alterations and ensure accurate analysis, samples were immediately preserved following collection. For the determination of reduced iron, as well as major and trace cations, concentrated nitric acid (1% by volume) was added to each sample. Once the samples were completely degassed, this acidity avoided the possibility of dissolved species precipitating during storage. All fluid samples were visually examined prior to analysis, and no precipitates were identified. Our experience has shown that gathering several samples in this way, along with prompt preservation and critical parameter analysis, yields a precise illustration of the in situ fluid composition.

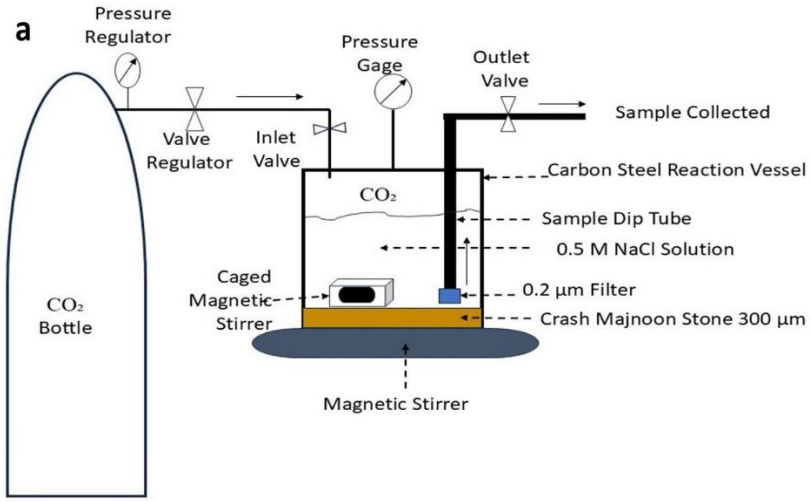

Figure 4. Batch reactor of reaction Majnoon rock stone with carbon dioxide

Experimental Setup and Procedure

The technique of X-ray diffraction (XRD) was used to perform quantitative mineralogical characterization of the samples before and after reaction with CO2. Using Cu Kα radiation at 40 kV and 40 mA, the analysis was conducted out on an AL-2700B diffractometer (Dandong Radiative Instruments Group Co., Ltd.) with a scanning range of 2θ from 10° to 70° in ambient conditions. A Scanning Electron Microscope (SEM) Inspect S-50 (Thermo Fisher Scientific, USA) running at an accelerating voltage of 25–30 kV was used to analyze the samples' morphology. The Majnoon rock stone samples were treated with a small layer of gold to improve electrical conductivity prior to SEM photography.

Results and Discussion

Scanning Electron Microscope (SEM)

Fine-grained quartz and feldspar grains make up the majority of the Majnoon rock stone sample, which is categorized as arenite. Diagenetic carbonate minerals, primarily calcite and dolomite, with calcite being the more prevalent phase, cement these grains (Figure 5). The EDX data shown in Figure 6 and Table 1 provide additional evidence for these mineralogical observations. The primary components of quartz are silicon and oxygen, which combine to generate silicon dioxide (SiO_2) (Kubota, 2003). A continuous framework of silicon-oxygen tetrahedra, consisting of billions of interconnected silicon and oxygen atoms, makes up each quartz crystal. There may also be trace amounts of contaminants, which could affect the hue of the material. The identification of quartz in the specimen was supported by the EDX investigation, which verified the presence of silicon and oxygen in the Majnoon rock stone sample.

Feldspars, which have the formula AT_4O_4, are made up of a number of minerals whose A symbols include K, Na, Ca, and T, which stand for Si and Al elements, with a ratio of 3:1 to 1:1 (Silva et al., 2019). The Majnoon rock stone specimen contains Na, Ca, Si, and Al, which are consistent with the existence of feldspar minerals, as shown by the EDX results in Figure 6 and Table 1. The most stable phase of calcium carbonate, calcite is mostly constituted of calcium carbonate ($CaCO_3$) and is frequently found in a variety of rock types and geological formations (Moore, 2001). The identification of calcite as a cementing phase is supported by the EDX data (Figure 6 and Table 1), which also verify the presence of calcium and oxygen in the Majnoon rock stone sample from the Majnoon field.

The main component of dolomite is calcium magnesium carbonate, which has the chemical formula $CaMg(CO_3)_2$ (Schwab, 2003). It can be found as a mineral and as a sedimentary rock, usually with roughly equal amounts of calcium and magnesium carbonate. Other minerals and contaminants may also be present in trace concentrations in dolomite. The identification of dolomite inside the cementing matrix was supported by the EDX study shown in Figure 6 and Table 1, which verified the presence of calcium, magnesium, carbon, and oxygen in the Majnoon rock stone sample from the Majnoon field.

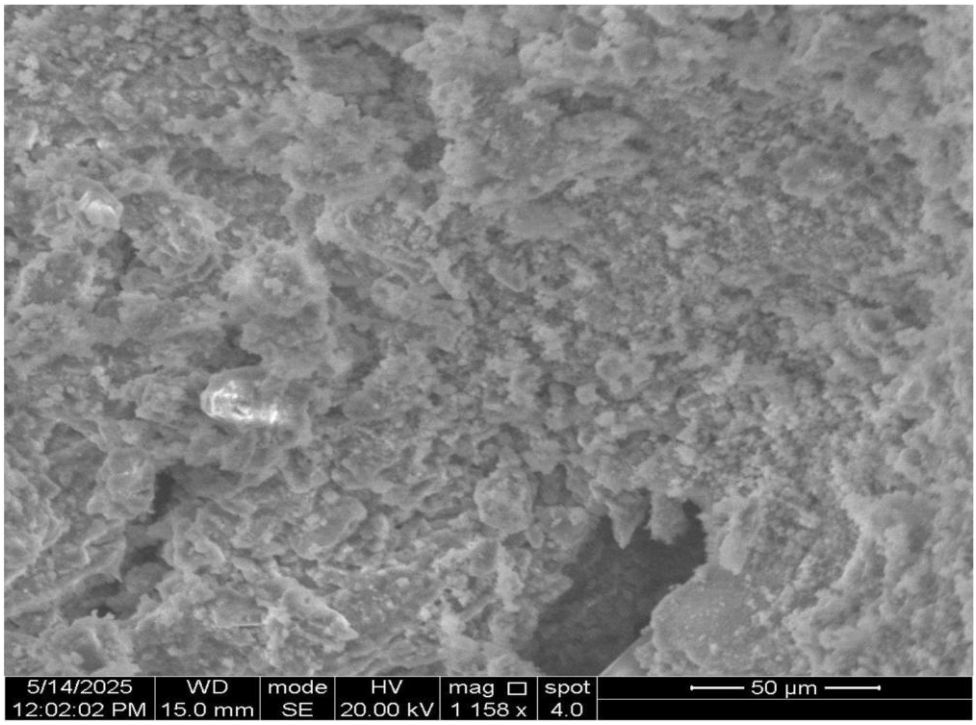

Figure 5. SEM images of an uncrushed sample of the Majnoon field

Table 1. The EDX test yielded the weight percentage of the components in the Majnoon field rock stone

Elements	Weight percent (wt%)
Carbon	31.29
Oxygen	31.94
Calcium	13.42
Sodium	4.87
Chlorine	3.03
Antimony	12.58
Ruthenium	1.45
Silicon	0.25
Fluorine	0.86
Magnesium	0.31

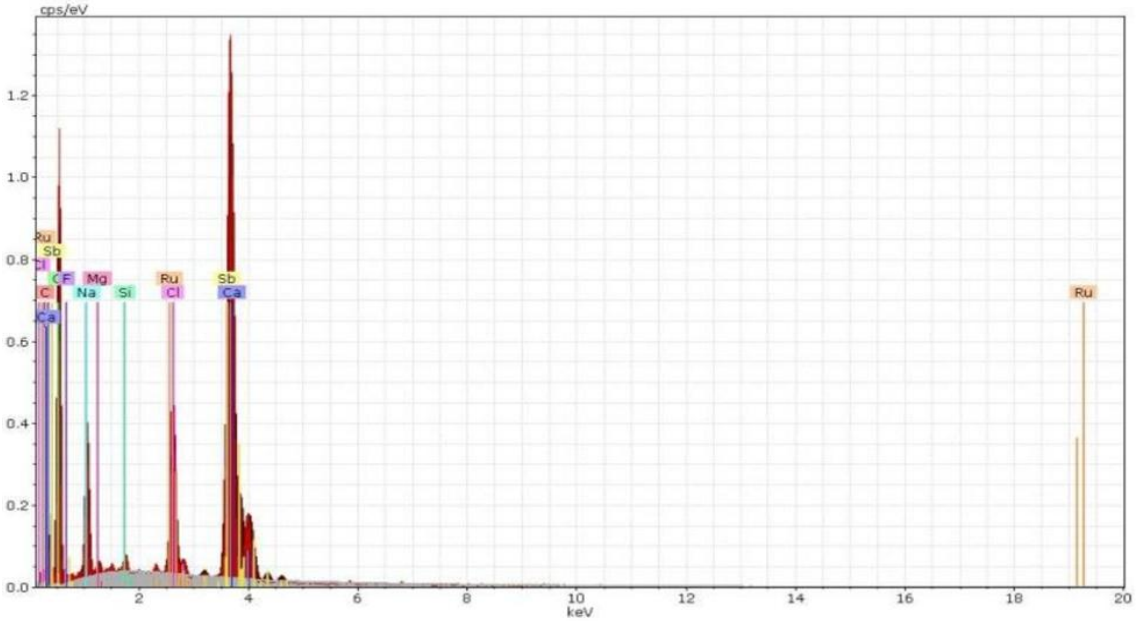

Figure 6. The EDX test of the Majnoon field rock stone

X-ray Diffraction (XRD)

The microscopic (SEM) observations were validated by XRD analysis, which showed that the sample has a typical mineralogical composition. Figure 7 and Table 2 show the outcomes for both unreacted and reacted samples. The Majnoon oil field rocks are mostly composed of albite, calcite, quartz, feldspars, clinochlore, dolomite, kaolinite, muscovite, orthoclase, and ankerite; phyllosilicates are found in smaller amounts. The following formulas were used to determine the weight percentages of each mineral phase as well as their percentage changes after interaction with CO2:

1) Weight Percentage of Each Phase: Calculated using the Reference Intensity Ratio (RIR) approach, as reported by Snyder and Bish (1989), Young (1993), Klug and Alexander (1974), and Chung (1974).
2)

$$W_i = \frac{\frac{I_i}{R_i\, RI}}{\Sigma \frac{I_j}{R_j\, RI}}\, x\, 100$$

Where:
W_i : Weight percentage of phase *i*
I_i : Intensity (or integrated area) of the main peak of phase *i*
j: Index running over all detected phases
RIRi: Reference Intensity Ratio of phase *i*, typically relative to corundum (Al_2O_3) as shown in Table 3.

3) Reaction Percentage of Each Phase*:* Determined following the methodologies outlined by Moore and Reynolds Jr. (1997), Brindley and Brown (1980), Środoń (2006), and the U.S. EPA Method (2001).

$$R\% = \frac{I_{initial} - I_{final}}{I_{initial}}\, x\, 100$$

Where:
$I_{initial}$: Intensity of the characteristic XRD peak of the mineral before the reaction.
I_{final}: Intensity of the same peak after the reaction.
R%: Phase percentage of reaction.

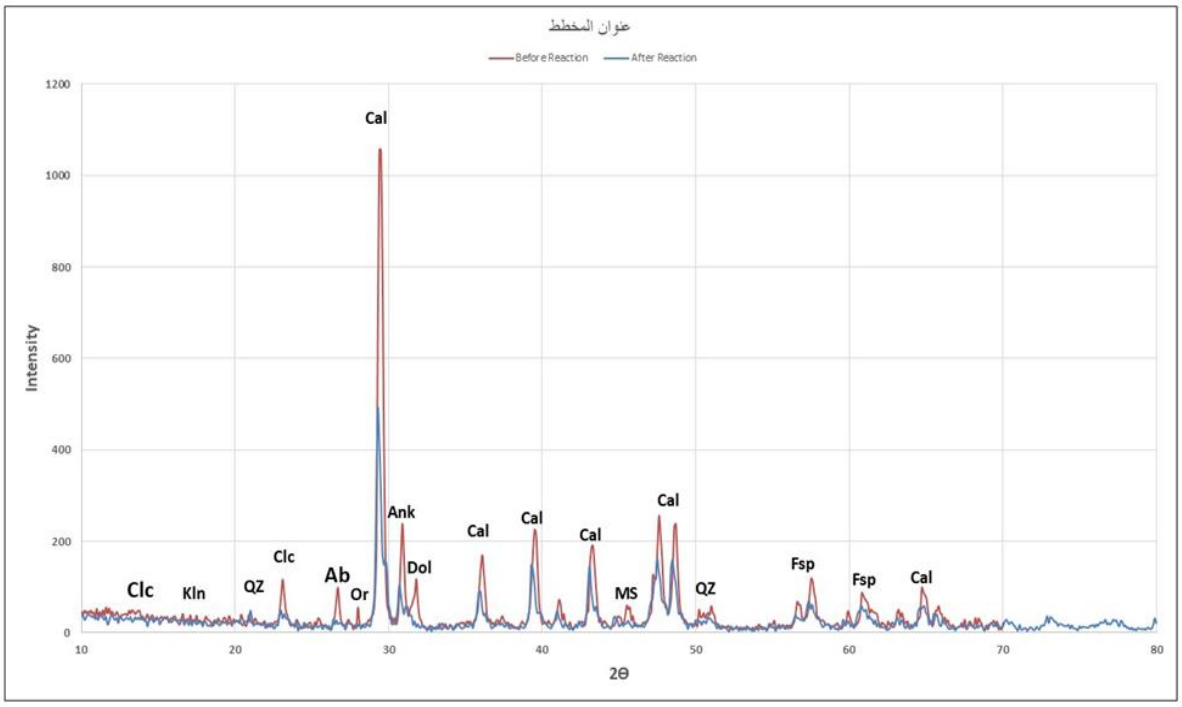

Figure 7. XRD patterns of the Majnoon rock stone sample prior and after the sCO2 reaction (at 87 days). Qz = quartz, Or = orthoclase, Ab = albite, Cal = calcite, Kln = kaolinite, Dol = dolomite, Ms = muscovite, Ank = ankerite, Clc = clinochlore, Fsp = feldspars

Table 2. Weight reaction percentage and quantitative X-ray analysis (wt%) of the samples prior to and following the reaction (at 87 days) with CO2-saturated brine

Minerals	Unreacted Sample	CO_2-reacted sample	Reaction Percentage
Clinochlore	3.802478	3.068586	56.55172
Kaolinite	0.770985	1.227435	14.28571
Quartz	6.380104	8.939649	24.5614
Albite	1.817322	0.613717	81.81818
Orthoclase	1.389163	0.414674	83.92857
Calcite	66.72452	69.76099	43.71041
Ankerite	8.12458	6.566523	56.48536
Dolomite	3.800178	2.931009	58.47458
Muscovite	0.969793	0.64331	64.28571
Feldspars	6.220913	5.834103	49.5082

Table 3. Reference intensity ratio (RIRi) of phases (Klug and Alexander, 1974; Chung 1974; Bish and Post, 1989; Moore and Reynolds, 1997)

Materials	Albite	Calcite	Quartz	Feldspars	Clinochlore	Dolomite	Kaolinite	Muscovite	Orthoclase	Ankerite
RIRi	5.00	3.04	0.82	3.5-5.5	3.5	2.85	2-3	5.3	3.7	2.7

As shown in Figure 7 and Table 2, the Majnoon rock stone sample contains several minerals—including albite, calcite, quartz, feldspars, clinochlore, dolomite, kaolinite, muscovite, orthoclase, and ankerite—with varying weight percentages. Before reaction, calcite exhibited the highest weight percentage at approximately 67%, while kaolinite had the lowest, around 0.77%. After reaction with CO_2, the weight percentages of the phases are also detailed in Table 2, with calcite again showing the highest value at approximately 69.67%, and orthoclase the lowest at about 0.41%.

Throughout the studies, exposure to CO2-saturated brine caused very slight mineralogical changes, according to a comparison of the weight percentages before and after the reaction. The comparatively slow reaction kinetics at the observed temperature are consistent with this small change. Changes in the relative proportions of carbonate phases and minor reductions in the amounts of albite and orthoclase are noteworthy. The incongruent dissolution of feldspars and phyllosilicates may be responsible for minor differences in other mineral phases, which could result in the creation of clay minerals (Black et al., 2014; Kaszuba et al., 2013).

Furthermore, following exposure to CO2, the reaction percentages of albite, calcite, quartz, feldspars, clinochlore, dolomite, kaolinite, muscovite, orthoclase, and ankerite phases are shown in Table 2, indicating different levels of reactivity. Albite and orthoclase showed the highest reaction percentages, at roughly 82% and 84%, respectively. On the other hand, at about 14% and 24%, respectively, kaolinite and quartz showed the lowest reaction percentages.

The following is a summary of each mineral phase's reaction equations and end products:
Every reaction is predicated on the idea that CO_2 dissolves in water to produce carbonic acid (H_2CO_3), which then splits into H^+ and HCO_3^- ions to aid in the dissolving and modification of minerals.

1. Albite ($NaAlSi_3O_8$)

Albite reacts with CO_2-saturated brine to form kaolinite, dawsonite, or amorphous silica, depending on environmental conditions such as temperature and pH (Xu et al., 2004; Gysi & Stefánsson, 2012; Palandri & Kharaka, 2004).

$$2NaAlSi_3O_8 + 2CO_2 + 11H_2O \rightarrow Al_2Si_2O_5(OH)_4 + 4H_4SiO_4 + 2Na^+ + 2HCO_3^-$$

Albite + CO_2 → Kaolinite + Silica + Ions

2. Calcite ($CaCO_3$)

Calcite is one of the most reactive minerals with CO_2 and readily dissolves in acidic, CO_2-rich fluids (Arvidson & Mackenzie, 1999).

$$CaCO_3 + CO_2 + H_2O \rightarrow Ca^{2+} + 2HCO_3^-$$

3. Quartz (SiO_2)

Quartz exhibits no direct reactivity with CO_2 and dissolves very slowly as silicic acid (Pokrovsky & Schott, 2001; Kaszuba et al., 2005).

$$SiO_2 + 2H_2O \rightleftharpoons H_4SiO_4$$

4. K-Feldspar / Orthoclase ($KAlSi_3O_8$)

Potassium and sodium feldspars undergo slow weathering reactions with CO_2 and H_2O, forming clay minerals and releasing alkalinity (Hellmann et al., 2012; Xu et al., 2004; Palandri & Kharaka, 2004).

$$2KAlSi_3O_8 + 2CO_2 + 11H_2O \rightarrow Al_2Si_2O_5(OH)_4 + 4H_4SiO_4 + 2K^+ + 2HCO_3^-$$
Orthoclase + CO_2 → Kaolinite + silicic acid + ions

5. Clinochlore ($(Mg,Fe)_5Al(Si_3Al)O_{10}(OH)_8$)

Clinochlore remains stable under many CO_2 storage conditions but may undergo slight transformation into other clay minerals (Pokrovsky et al., 2005).

$$(Mg_5Al)(Si_3Al)O_{10}(OH)_8 + 10H^+ \rightarrow 5Mg^{2+} + Al^{3+} + 3SiO_2 + H_2O$$

6. Dolomite ($CaMg(CO_3)_2$)

Dolomite dissolves in CO_2-rich fluids more slowly than calcite but still at a significant rate; under certain conditions, it may also reprecipitate (Arvidson & Mackenzie, 1999; Gunter et al., 2000).

$$CaMg(CO_3)_2 + 2CO_2 + 2H_2O \rightarrow Ca^{2+} + Mg^{2+} + 4HCO_3^-$$
Dolomite → ions → bicarbonate.

7. Kaolinite ($Al_2Si_2O_5(OH)_4$)

Generally, kaolinite is considered stable; however, under elevated CO_2 pressure and temperature, it can slowly undergo dissolution or transformation (Carroll & Knauss, 2005; Gysi & Stefánsson, 2012).

$$Al_2Si_2O_5(OH)_4 + 6H^+ \rightarrow 2Al^{3+} + 2H_4SiO_4 + H_2O$$

8. Muscovite ($KAl_2(AlSi_3O_{10})(OH)_2$)

Muscovite exhibits very low reactivity with CO_2 and remains stable under most geological storage conditions (Brantley et al., 2008; Pokrovsky & Schott, 2001).

$$KAl_2(AlSi_3O_{10})(OH)_2 + 6H^+ \rightarrow K^+ + 3Al^{3+} + 3SiO_2 + H_2O$$

9. Ankerite ($Ca(Fe,Mg)(CO_3)_2$)

Ankerite behaves similarly to dolomite; it dissolves in CO_2-rich fluids and may reprecipitate as secondary carbonate minerals (Kaszuba et al., 2005; Gunter et al., 2000).

$$Ca(Fe,Mg)(CO_3)_2 + 2CO_2 + 2H_2O \rightarrow Ca^{2+} + Fe^{2+} + Mg^{2+} + 4HCO_3^-$$
Ankerite → ions → bicarbonate.

Previous CO2–water–rock interaction studies have provided substantial documentation of the dissolution and modification of carbonate minerals as well as the concurrent hydrolysis of aluminosilicates, especially feldspars into clays (Kaszuba et al., 2013; Lu et al., 2013; Wigand et al., 2008). For example, mineralogical studies at the

Wekerdam gas field showed that dolomite and siderite were the main carbonate precipitates, while feldspar hydrolysis promoted the conversion of kaolinite into illite (Koenen et al., 2013). Similarly, under reservoir-like conditions (T = 100°C, P = 24 MPa), laboratory tests on sandstone samples from China's Songliao Basin showed full calcite dissolution and partial feldspar hydrolysis, along with an enrichment in quartz and clay minerals (Yu et al., 2012).

The significance of CO2–feldspar reactions and the resulting formation of clay minerals is supported by findings from higher-temperature studies—up to 200°C—on both sandstones (Kaszuba et al., 2003; Lu et al., 2013) and granite (Lin et al., 2008), even though the current study operated at temperatures below 100°C. Interestingly, despite the fact that dawsonite is a theoretically conceivable byproduct of feldspar hydrolysis in sodium-rich fluids, none of these earlier investigations documented its precipitation (De Silva et al., 2015):

$$\underset{\text{Albite}}{NaAlSi_3O_8} + CO_2 + H_2O \rightarrow \underset{\text{Dawsonite "amorphous"}}{NaAlCO_3(OH)_2} + 3SiO_2$$

Because of its relatively large molar volume, which may affect reservoir porosity and permeability, Dawsonite has been regarded as an important secondary mineral phase in many geochemical modeling studies (Johnson et al., 2004). In certain sandstone formations exposed to CO2 at high temperatures and pressures, empirical evidence of dawsonite formation has been shown (Worden, 2006; Zhou et al., 2014). Its precipitation has been connected to interactions with acidic, high-salinity brines in some situations (Worden, 2006) and to the presence of alkaline Na–HCO_3-rich fluids in others (Kampman et al., 2014).

However, it is still uncertain if dawsonite actually occurs in natural and artificial environments. Even in controlled laboratory studies using pure feldspar samples, its development has frequently been predicted but not observed (Alemu et al., 2011; Gaus et al., 2005; Huq et al., 2012; Van Pham et al., 2011; Wigand et al., 2008). Further concerns about the conditions necessary for its stability have been highlighted by the fact that it appears to be absent in many natural CO2-rich environments (Hellevang et al., 2011). Kinetic constraints, insufficiently high temperatures, or low pH levels that could prevent its nucleation and growth are possible reasons for its absence (Hellevang et al., 2011; Lu et al., 2013).

Fluid Chemistry

Table 4 summarizes the concentrations of the primary ions and specific elements from the experimental runs, including data for the brine after 37 days of saturation (CO_2-free) and another 50 days under CO_2-saturated circumstances (a total of 87 days). After CO2 injection, there was a discernible alteration in the chemistry of the solution. In particular, the dissolution of CO2 in water caused the pH of the initial solution to drop considerably, which resulted in the creation of an acidic solution by the following reaction:

$$CO2(g) + H2O(l) \rightleftharpoons H2CO3(aq) \rightleftharpoons H + (aq) + HCO3 - (aq)$$

This acidity promotes geochemical processes between the brine and rock matrix, improves mineral dissolution, and modifies elements concentrations.

Table 4. Analyzing the collected fluids chemically

Analyte	Brine with after 37 days	Brine with sCO_2 after 87 days
pH(at 24°C) (mgL^{-1})	7.62	6.61
Ca	70.6377	1190.205
Mg	7.1	45.129
K	5.442	6.0614
Si	3.676	22.897
Fe	0.0422	0.7197
Al	0.0224	0.699

It should be mentioned, too, that solutions that were mostly degassed by the time of analysis correlate to the measured pH values. Figure 8 shows the key element chemical development of the extracted fluid samples, and Table 4 provides a summary. Ion concentrations somewhat increased after the first brine–Majnoon rock stone interaction, most likely as a result of carbonate mineral dissolution and possible ion exchange processes taking

place on clay mineral surfaces. Significantly, concentrations of silicon and aluminum reached 3.676 mg/L and 0.0224 mg/L, respectively, demonstrating a little breakdown of aluminosilicate, specifically muscovite and clinochlore. The partial dissolution of clinochlore or ankerite within the Majnoon rock stone matrix may be the cause of the low but detectable quantities of dissolved iron (up to 0.0422 mg·L⁻¹) found.

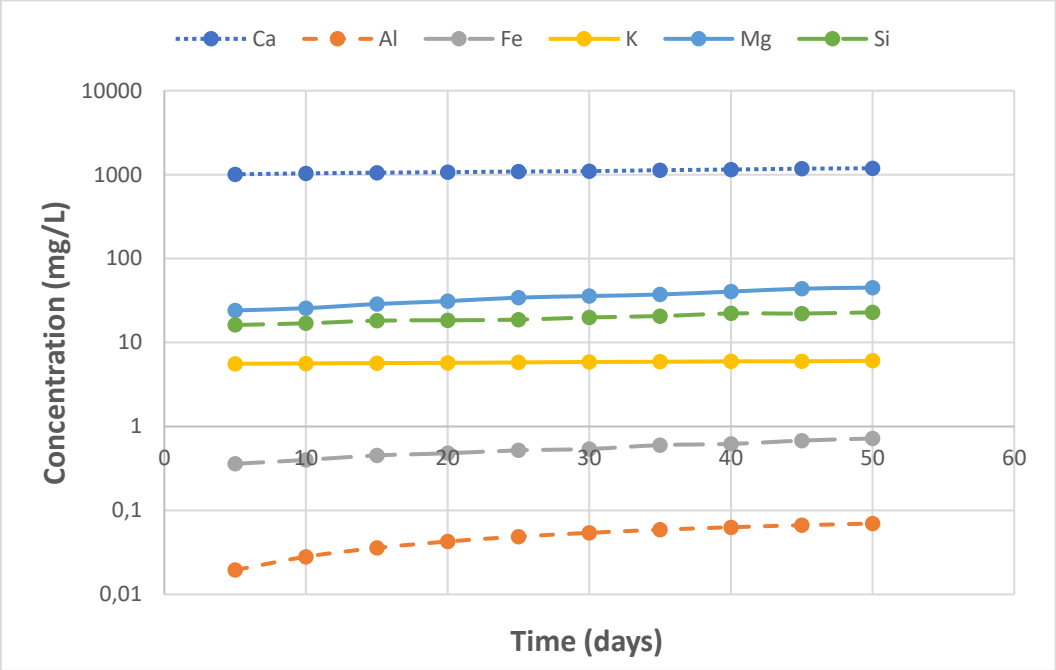

Figure 8. Fluid sample measurement of chemical data as a function of time

Ion concentrations were observed to have significantly increased after CO2 was added to the reaction vessel. Brine acidification and the consequent decomposition of calcite and dolomite were the main causes of the significant increase in calcium concentrations, which reached about 1009 mg·L⁻¹ within the first five days. In the Majnoon rock stone trials, potassium concentrations rose to about 5.59 mg·L⁻¹, primarily due to muscovite hydrolysis. Throughout the trial, the concentrations of silicon and magnesium showed a consistent rising trend. Iron and aluminum concentrations, on the other hand, only slightly rose. The weak kinetics of degradation events under low-temperature settings, which limit their quantification during the very short experimental period (a few months), are probably the cause of this limited mobilization (Gaus, 2010).

By about day 50 of the experiment, the ion concentrations in solution had generally reached a quasi-steady state. This finding is in line with earlier research by Kaszuba et al. (2003), who saw comparable behavior after ~55 days at 200°C and 200 pressure, and Wigand et al. (2008), who documented stability after ~33 days at 60°C and 150 bar. It should be mentioned that, through concentration effects, the gradual decrease in the brine-to-rock ratio brought about by frequent fluid sampling may have led to ion enrichment in the finished solution. The following reactions are suggested to explain the observed fluid-rock interactions by combining the mineralogical and geochemical data:

i. *Dissolution of carbonates:*
Calcium (Ca^{2+}), magnesium (Mg^{2+}), and bicarbonate (HCO_3^-) ions were released into the solution when calcite and dolomite in the Majnoon rock stone sample interacted with the CO_2-saturated brine. The overall response can be expressed as follows:

$$\underset{\text{Calcite}}{CaCO_3} + \underset{\text{Dolomite}}{CaMg(CO_3)_2} + 3H^+ \rightarrow 2Ca^{+2} + Mg^{+2} + 3HCO_3^-$$

As a possible alternative, a partial dissolution and reprecipitation transformation from ankerite to dolomite has been suggested; this reaction is represented by the following:

$$\underset{\text{Ankerite}}{CaFe_{0.4}Mg_{0.6}(CO_3)_2} + 0.8H^+ \rightarrow 0.4Ca^{+2} + 0.4Fe^{+2} + 0.6\underset{\text{Dolomite}}{CaMg(CO_3)_2} + 0.8HCO_3^-$$

As calcium concentrations reached a steady state rapidly—within approximately 5 days after CO_2 injection, as shown in Figure 8—it was inferred that the observed excess magnesium concentration originated from a different source. This suggests that ankerite reacts with carbonic acid (H_2CO_3) to form dolomite. Subsequently, dolomite further dissolves in the acidic environment, alongside calcite dissolution, contributing to the elevated magnesium ion concentration observed in the brine solution.

ii. Hydrolysis of phyllosilicates (clinochlore/muscovite):

Numerous research (e.g., Alemu et al., 2011; Black et al., 2014; Luquot et al., 2012) supported the theory that the excess magnesium content was caused by the hydrolysis of clinochlore. Gaus (2010) states that the following reaction pathway can occur when chlorite interacts with calcite and dissolved CO2 to form siderite, dolomite, kaolinite, and amorphous silica:

$$\underset{\text{Chlorite}}{Fe_{2.5}Mg_{2.5}Al_2Si_3O_{10}(OH)_8} + 2.5\underset{\text{Calcite}}{CaCO_3} + 5CO_2 \rightarrow$$

$$2.5\underset{\text{Siderite}}{FeCO_3} + 2.5\underset{\text{Dolomite}}{CaMg(CO_3)_2} + \underset{\text{Kaolinite}}{Al_2Si_2O_5(OH)_4} + \underset{\text{“Chalcedony”}}{SiO_2} + 2H_2O$$

In our study, calcite and dolomite dissolved in the Majnoon field rock stone sample, while siderite was not detected, as confirmed by the EDX analysis (Table 1). Additionally, the mass of kaolinite remained nearly unchanged; Table 2 shows only a minor difference in its weight percentage before and after the reaction, with the lowest reaction percentage among all phases. Even if the proposed reaction involving chlorite hydrolysis had occurred, the small amounts of resulting minerals would likely be below the detection limits of the employed methods (XRD and SEM). Potassium release is likely due to minor muscovite dissolution in the brine. The relatively stable potassium concentration during CO_2 diffusion, as shown in Figure 8 and Table 4, suggests minimal further interaction of muscovite with the solution.

iii. Precipitation of montmorillonite:

In several studies, montmorillonite formation has been directly linked to the hydrolysis of albite (Fischer et al., 2011; Huq et al., 2012; Wigand et al., 2008). A simplified reaction for this process can be expressed as:

$$\underset{\text{Albite}}{2NaAlSi_3O_8} + 2CO_2 + 2H_2O \rightarrow \underset{\text{Montmorillonite}}{Al_2Si_4O_{10}(OH)_2} + 2Na^+ + 2SiO_2 + 2HCO_3^-$$

Table 2 illustrates how the mass of albite changed dramatically, with a reaction percentage of 81.82% and a weight percentage drop of 1.2%. This suggests that as albite was reduced, montmorillonite emerged in the sample. Consequently, it makes sense to assume that montmorillonite is a byproduct of the hydrolysis of albite. These responses are in line with earlier research on siliciclastic formations and were verified both experimentally and numerically (Horner et al., 2015; Huq et al., 2015).

Conclusions

Under simulated reservoir conditions (T = 60°C, P = 74bar, over 87 days in batch experiments), this study analyzed the geochemical interactions between Majnoon rock stone specimens from the Majnoon Field (Iraq) and CO2. Albite, calcite, quartz, feldspars, clinochlore, dolomite, kaolinite, muscovite, orthoclase, and ankerite formed the majority of the Majnoon rock stone. According to mXRD analysis, calcite had the highest weight percentage both before and after CO2 exposure, while kaolinite and orthoclase showed the lowest percentages, respectively. CO_2-saturated brine led to increasing quantities of dissolved cations, indicating mineral dissolution. Overall, though, the mineralogical alterations were not very significant. Significantly, the amounts of orthoclase and albite dropped, whereas the carbonate phases varied only slightly. The reactions involved included carbonate dissolution, hydrolysis of phyllosilicates (clinochlore and muscovite), and the formation of montmorillonite. Albite and orthoclase exhibited the highest reactivity with CO_2, while kaolinite and quartz were the least reactive. Montmorillonite was observed to form as a secondary phase, likely resulting from albite hydrolysis.

Recommendations

Further studies should test the reaction of CO_2 with Majnoon rock in situ field. Moreover, the study can be applied to another field of oil. In addition, it can be used with other acids to replace the CO_2.

Scientific Ethics Declaration

* The authors declare that the scientific, ethical, and legal responsibility of this article published in EPSTEM journal belongs to the authors.

Conflict of Interest

* The authors declare that they have no conflicts of interest

Funding

* This work did not receive any specific grant from funding agencies.

Acknowledgements or Notes

* This article was presented as an oral presentation at the International Conference on Engineering and Advanced Technology (ICEAT) held in Selangor, Malaysia on July 23-24, 2025.

References

Al-Ameri, T. K., Zumberge, J., & Markarian, Z. M. (2011). Hydrocarbons in the Middle Miocene Jeribe Formation, Dyala region, NE Iraq. *Journal of Petroleum Geology*, *34*(2), 199–216.

Alemu, B. L., Aagaard, P., Munz, I. A., & Skurtveit, E. (2011). Caprock interaction with CO2: A laboratory study of reactivity of shale with supercritical CO2 and brine. *Applied Geochemistry*, *26*, 1975–1989.

Arvidson, R. S., & Mackenzie, F. T. (1999). The dolomite problem: Control of precipitation kinetics by temperature and saturation state. *American Journal of Science*, *299*(4), 257–288.

Atreya, A. A. (2022). *Feasibility study of carbon capture and storage process to implement in maritime industry* (Master's thesis) UiT Arctic University of Norway.

Baraka, A. (2015). Investigation of temperature effect on surface-interaction and diffusion of aqueous-solution/porous-solid adsorption systems using diffusion-binding model. *Journal of Environmental Chemical Engineering*, *3*, 129–139.

Bateman, K., Turner, G., Pearce, J. M., Noy, D. J., Birchall, D., & Rochelle, C. A. (2005). Large scale column experiment: Study of CO2, porewater, rock reactions and model test case. *Oil & Gas Science and Technology*, *60*, 161–175.

Bish, D. L., & Post, J. E. (1989). *Modern powder diffraction*. Mineralogical Society of America.

Black, J. R., Carroll, S. A., & Haese, R. R. (2014). Rates of mineral dissolution under CO2 storage conditions. *Chemical Geology*, *399*, 134–144.

Brantley, S. L., White, A. F., & Kubicki, J. D. (Eds.). (2008). *Kinetics of water-rock interaction*. Springer.

Brindley, G. W., & Brown, G. (1980). *Crystal structures of clay minerals and their X-ray identification*. Mineralogical Society.

Bruhn, T., Naims, H., & Olfe-Kräutlein, B. (2016). Separating the debate on CO2 utilisation from carbon capture and storage. *Environmental Science & Policy*, *60*, 38–43.

Bureau of Environment Tokyo Metropolitan Government. (2019). *Final energy consumption and greenhouse gas emissions in Tokyo, 2019*. https://www.kankyo1.metro.tokyo.lg.jp/archive/en/climate/index.files/Tokyo_GHG_2019.pdf

Carroll, S. A., & Knauss, K. G. (2005). Dependence of labradorite dissolution kinetics on CO2(aq), Al(aq), and temperature. *Chemical Geology*, *217*(3–4), 213–225.

Chung, F. H. (1974). Quantitative interpretation of X-ray diffraction patterns of mixtures. I. Matrix-flushing method for quantitative multicomponent analysis. *Journal of Applied Crystallography*, *7*, 519–525.

Climate Action Tracker. (2023). *Countdown to COP28: Time for world to focus on oil and gas phase-out, renewables target - not distractions like CCS*. Retrieved from https://climateactiontracker.org/publications/countdown-to-COP28/

De Silva, G. P. D., Ranjith, P. G., & Perera, M. S. A. (2015). Geochemical aspects of CO2 sequestration in deep saline aquifers: A review. *Fuel*, *155*, 128–143.

European Commission. (2024). *Towards an ambitious industrial carbon management for the EU*. https://eur-lex.europa.eu/legal-content/EN/TXT/HTML/?uri=CELEX:52024DC0062

Evar, B., Armeni, C., & Scott, V. (2012). An introduction to key developments and concepts in CCS: History, technology, economics and law. In N. Markusson, S. Shackley, & B. Evar (Eds.), *Social dynamics of carbon capture and storage* (pp. 18–30). Routledge.

Fischer, S., Zemke, K., Liebscher, A., & Wandrey, M. (2011). Petrophysical and petrochemical effects of long-term CO2-exposure experiments on brine-saturated reservoir sandstone. *Energy Procedia*, *4*, 4487–4494.

Galarza, C., Buil, B., Peña, J., Martín, P. L., Gómez, P., & Garralón, A. (2013). Preliminary results from the experimental study of CO2-brine-rock interactions at elevated T & P: Implications for the pilot plant for CO2 storage in Spain. *Procedia Earth and Planetary Science*, *7*, 272–275.

García-Rios, M., Luquot, L., Soler, J. M., & Cama, J. (2013). Laboratory-scale interaction between CO2-rich brine and reservoir rocks (limestone and sandstone). *Procedia Earth and Planetary Science*, *7*, 109–112.

Gaus, I. (2010). Role and impact of CO2-rock interactions during CO2 storage in sedimentary rocks. *International Journal of Greenhouse Gas Control*, *4*, 73–89.

Gaus, I., Le Guern, C. C., Pearce, J., Pauwels, H. H., Shepherd, T., Hatziyannis, G., Metaxas, A., & Hatziynnis, G. (2005). Comparison of long-term geochemical interactions at two natural CO2-analogues: Montmiral (Southeast basin, France) and Messokampos (Florina basin, Greece) case studies. *Proceedings of the 7th International Conference on Greenhouse Gas Control Technologies*, 561–569.

Gunter, W. D., Perkins, E. H., & Hutcheon, I. (2000). Aquifer disposal of acid gases: Modeling of water–rock reactions for trapping of acid wastes. *Environmental Geosciences*, *7*(2), 73–90.

Gysi, A. P., & Stefánsson, A. (2012). Mineralogical aspects of CO2 sequestration during hydrothermal basalt alteration—An experimental study at 75 to 250 °C and elevated pCO2. *Chemical Geology*, *306–307*, 146–159.

Hellevang, H., Declercq, J., & Aagaard, P. (2011). Why is dawsonite absent in CO2 charged reservoirs? *Oil & Gas Science and Technology – Revue d'IFP Energies Nouvelles*.

Hellmann, R., Wirth, R., Daval, D., Barnes, J. P., Penisson, J. M., Tisserand, D., ... & Morin, G. (2012). The role of nanoscale interfacial dissolution–precipitation processes in the slow failure of silicate minerals. *Geochimica et Cosmochimica Acta*, *77*, 282–294.

Horner, K. N., Schacht, U., & Haese, R. R. (2015). Characterizing long-term CO2-water-rock reaction pathways to identify tracers of CO2 migration during geological storage in a low-salinity, siliciclastic reservoir system. *Chemical Geology*, *399*, 123–133.

Huq, F., Blum, P., Marks, M. A. W., Nowak, M., Haderlein, S. B., & Grathwohl, P. (2012). Chemical changes in fluid composition due to CO2 injection in the Altmark gas field: Preliminary results from batch experiments. *Environmental Earth Sciences*, *67*, 385–394.

Huq, F., Haderlein, S. B., Cirpka, O. A., Nowak, M., Blum, P., & Grathwohl, P. (2015). Flow through experiments on water-rock interactions in a sandstone caused by CO2 injection at pressures and temperatures mimicking reservoir conditions. *Applied Geochemistry*, *58*, 136–146.

International Energy Agency. (2021). *About CCUS*. Retrieved from https://www.iea.org/reports/about-ccus

International Energy Agency. (2022). *CO2 emissions reductions in the sustainable development scenario relative to the stated policies scenario*. Retrieved from https://www.iea.org/data-and-statistics/charts/co2-emissions-reductions-in-the-sustainable-development-scenario-relative-to-the-stated-policies-scenario-2019-2030

Johnson, J. W., Nitao, J., & Knauss, K. G. (2004). Reactive transport modelling of CO2 storage in saline aquifers to elucidate fundamental processes, trapping mechanisms, and sequestration partitioning. *Geological Society, London, Special Publications*, *233*, 107–128.

Kampman, N., Bickle, M., Wigley, M., & Dubacq, B. (2014). Fluid flow and CO2-fluid-mineral interactions during CO2-storage in sedimentary basins. *Chemical Geology*, *369*, 22–50.

Kaszuba, J. P., Janecky, D. R., & Snow, M. G. (2003). Carbon dioxide reaction processes in a model brine aquifer at 200°C and 200 bars: Implications for geologic sequestration of carbon. *Applied Geochemistry*, *18*, 1065–1080.

Kaszuba, J. P., Janecky, D. R., & Snow, M. G. (2005). Experimental evaluation of mixed fluid reactions between supercritical carbon dioxide and NaCl brine: Relevance to the integrity of a geologic carbon repository. *Chemical Geology*, *217*(3–4), 277–293.

Kaszuba, J. P., Yardley, B. W. D., & Andreani, M. (2013). Experimental perspectives of mineral dissolution and precipitation due to carbon dioxide-water-rock interactions. *Reviews in Mineralogy and Geochemistry*, *77*, 153–188.

Klug, H. P., & Alexander, L. E. (1974). *X-ray diffraction procedures for polycrystalline and amorphous materials* (2nd ed.). Wiley.

Koenen, M., Wasch, L. J., Van Zalinge, M. E., & Nelskamp, S. (2013). Werkendam, the Dutch natural analogue for CO2 storage — Long-term mineral reactions. *Energy Procedia*, *37*, 3452–3460.

Kubota, K. (2003). Quartz crystals for watches. In K. H. J. Buschow et al. (Eds.), *Encyclopedia of materials: Science and technology* (pp. 1–9). Elsevier.

Lin, H., Fujii, T., Takisawa, R., Takahashi, T., & Hashida, T. (2008). Experimental evaluation of interactions in supercritical CO2/water/rock minerals system under geologic CO2 sequestration conditions. *Journal of Materials Science*, *43*, 2307–2315.

Lu, P., Fu, Q., Seyfried, W. E., Hedges, S. W., Soong, Y., Jones, K., & Zhu, C. (2013). Coupled alkali feldspar dissolution and secondary mineral precipitation in batch systems - 2: New experiments with supercritical CO2 and implications for carbon sequestration. *Applied Geochemistry*, *30*, 75–90.

Luquot, L., Andreani, M., Gouze, P., & Camps, P. (2012). CO2 percolation experiment through chlorite/zeolite-rich sandstone (Pretty Hill Formation — Otway Basin, Australia). *Chemical Geology*, *294–295*, 75–88.

Moore, C. H. (2001). Concepts of sequence stratigraphy as applied to carbonate depositional systems. *Developments in Sedimentology*, *55*, 19–36.

Moore, D. M., & Reynolds, R. C. (1997). *X-ray diffraction and the identification and analysis of clay minerals* (2nd ed.). Oxford University Press.

Palandri, J. L., & Kharaka, Y. K. (2004). *A compilation of rate parameters of water–mineral interaction kinetics for application to geochemical modeling* (Open-File Report 2004–1068). U.S. Geological Survey.

Pokrovsky, O. S., & Schott, J. (2001). Experimental study of brucite dissolution and precipitation in aqueous solutions: Surface speciation and chemical affinity control. *Geochimica et Cosmochimica Acta*, *65*(6), 905–921.

Rathnaweera, T. D., Ranjith, P. G., & Perera, M. S. A. (2016). Experimental investigation of geochemical and mineralogical effects of CO2 sequestration on flow characteristics of reservoir rock in deep saline aquifers. *Scientific Reports*, *6*, 19362.

Schwab, F. L. (2003). Sedimentary petrology. In R. A. Meyers (Ed.), *Encyclopedia of physical science and technology* (3rd ed., pp. 495–529). Academic Press.

Silva, J. C., Ulsen, C., Bergerman, M. G., & Horta, D. G. (2019). Reduction of Fe2O3 content of foyaite by flotation and magnetic separation for ceramics production. *Journal of Materials Research and Technology*, *8*(5), 4915–4923.

Snyder, R. L., & Bish, D. L. (1989). Quantitative analysis of crystalline mixtures by the Rietveld method. *Reviews in Mineralogy*, *20*.

Sorensen, J. A., Holubnyak, Y. I., Hawthorne, S. B., Miller, D. J., Eylands, K., Steadman, E. N., & Harju, J. A. (2009). Laboratory and numerical modeling of geochemical reactions in a reservoir used for CO2 storage. *Energy Procedia*, *1*, 3391–3398.

Środoń, J. (2006). Interpretation of X-ray diffraction patterns of mixtures of clay minerals. *Clays and Clay Minerals*, *54*(6), 771–785.

U.S. EPA. (2001). *Characterization of minerals using XRD and Rietveld analysis* (Method 600/R-01/070).

Van Pham, T. H., Lu, P., Aagaard, P., Zhu, C., & Hellevang, H. (2011). On the potential of CO2-water-rock interactions for CO2 storage using a modified kinetic model. *International Journal of Greenhouse Gas Control*, *5*, 1002–1015.

Wigand, M., Carey, J. W., Schütt, H., Spangenberg, E., & Erzinger, J. (2008). Geochemical effects of CO2 sequestration in sandstones under simulated in situ conditions of deep saline aquifers. *Applied Geochemistry*, *23*, 2735–2745.

Worden, R. H. (2006). Dawsonite cement in the Triassic Lam Formation, Shabwa Basin, Yemen: A natural analogue for a potential mineral product of subsurface CO2 storage for greenhouse gas reduction. *Marine and Petroleum Geology*, *23*, 61–77.

Xu, T., Apps, J. A., & Pruess, K. (2004). *Numerical modeling of CO2 sequestration in geologic formations* (LBNL Report). Lawrence Berkeley National Laboratory.

Young, R. A. (1993). *The Rietveld method*. Oxford University Press.

Yu, Z., Liu, L., Yang, S., Li, S., & Yang, Y. (2012). An experimental study of CO2–brine–rock interaction at in situ pressure–temperature reservoir conditions. *Chemical Geology*, *326–327*, 88–101.

Zhang, M., & Pu, J. (2011). Mineral materials as feasible amendments to stabilize heavy metals in polluted urban soils. *Journal of Environmental Sciences*, *23*, 607–615.

Zhou, B., Liu, L., Zhao, S., Ming, X. R., Oelkers, E. H., Yu, Z. C., & Zhu, D. F. (2014). Dawsonite formation in the Beier Sag, Hailar Basin, NE China tuff: A natural analog for mineral carbon storage. *Applied Geochemistry*, *48*, 155–167.

Author(s) Information

Ibrahem I. Moslam
University of Al-Qadisiyah, Al-Diwaniyah City 58002, Iraq
Contact e-mail: *eng.Ibrahim1998th@gmail.com*

Ali A. Jazie
University of Al-Qadisiyah, Al-Diwaniyah City 58002, Iraq

Rafid K. Abbas
University of Al-Qadisiyah, Al-Diwaniyah City 58002, Iraq

To cite this article:

Moslam, I. I., Jazie, A. A., & Abbas, R. K. (2025). Characterization and properties of reaction Majnoon field rock stone with carbon dioxide. *The Eurasia Proceedings of Science, Technology, Engineering and Mathematics (EPSTEM), 37,* 720- 735.